2015

Porous amorphous Ge/C composites with excellent electrochemical properties

Xiu Li
Hunan University

Wei Guo
Anyang Normal University

Qian Wan
Hunan University

Jianmin Ma
University of Wollongong

Publication Details

Li, X., Guo, W., Wan, Q. & Ma, J. (2015). Porous amorphous Ge/C composites with excellent electrochemical properties. RSC Advances: an international journal to further the chemical sciences, 5 (36), 28111-28114.

Porous amorphous Ge/C composites with excellent electrochemical properties

Abstract
Porous amorphous germanium/carbon (Ge/C) composites, which were synthesized through the reduction/carbonization of germanium oxide/oleic acid precursors, could exhibit a high-capacity, high-rate and long-life performance due to the synergistic effect of the porous structure and carbon.

Keywords
excellent, composites, properties, c, electrochemical, ge, amorphous, porous

Publication Details
Li, X., Guo, W., Wan, Q. & Ma, J. (2015). Porous amorphous Ge/C composites with excellent electrochemical properties. RSC Advances: an international journal to further the chemical sciences, 5 (36), 28111-28114.

RSC Advances

COMMUNICATION

View Article Online
View Journal | View Issue

Cite this: RSC Adv., 2015, 5, 28111

Porous amorphous Ge/C composites with excellent electrochemical properties†

Xiu Li,[a] Wei Guo,*[b] Qian Wan[a] and Jianmin Ma*[ac]

Received 8th February 2015
Accepted 11th March 2015

DOI: 10.1039/c5ra02459e

www.rsc.org/advances

Porous amorphous germanium/carbon (Ge/C) composites, which were synthesized through the reduction/carbonization of germanium oxide/oleic acid precursors, could exhibit a high-capacity, high-rate and long-life performance due to the synergistic effect of the porous structure and carbon.

Recently, the demand for lithium-ion batteries (LIBs) with high energy/power density and long cycle life has been driven by the development of portable electronics.[1] To meet the demand, conversional anodes for LIBs (*i.e.*, graphite, $Li_4Ti_5O_{12}$) should be replaced by high-capacity anode materials, such as transition metal oxides (TMOs) and some element anodes (Si, P, Ge and Sn).[2–12] Compared to TMOs, element anodes (4200, 2596, 1600 and 994 mA h g^{-1} for corresponding Si, P, Ge and Sn) have a higher theoretical capacity. Among them, Ge is attracting attention due to high lithium diffusivity (400 times higher than that in Si) and high conductivity.[13] These merits make Ge attractive as a high-rate, high-capacity anode. However, their application is limited by their short cycling life due to the large volume changes (370% when fully lithiated to $Li_{4.4}Ge$) during lithium insertion and deinsertion.[14]

To solve this problem, many efforts have been made improve their cycling performance through facilitating strain relaxation, including morphological control, porous structure, carbon coating, and hybridizing with other components.[15–22] Among them, coating or hybridizing with carbon is the most effective way to protect Ge through embedding it in the carbon matrix.[23–30] Most of reported examples about Ge/C composites involve complicated procedures or special equipments.[31–33] Thus, easy fabrication of Ge/C composites is highly desired.

In this communication, we present the method of the thermo-reduction/carbonization of germanium oxide (GeO_2)/oleic acid precursors to synthesize the porous amorphous Ge/C composites. The as-obtained Ge/C composites have displayed to be the structure of Ge nanoparticles embedded in the carbon matrix. In virtue of this structure, the as-obtained porous amorphous Ge/C composites display long cycling life and good rate ability. The Ge/C composites could maintain a capacity of ~681 mA h g^{-1} after 350 cycles at a current density of 200 mA g^{-1}, and obtain a capacity of ~450 mA h g^{-1} at a current density of 6400 mA g^{-1}. The as-obtained porous amorphous Ge/C composites are promising anodes for next-generation LIBs.

The composite and structure of porous amorphous Ge/C composite was characterized by X-ray diffraction (XRD) technique. As shown in Fig. 1, all the peaks in the XRD pattern of the porous amorphous Ge/C composite could be well indexed with pure Ge (JCPDS card no. 04-0545). The absence peak of carbon in the XRD pattern of porous amorphous Ge/C composites is due to the existence of amorphous carbon. Thermogravimetric analysis (TGA) results in Fig. S1† show the

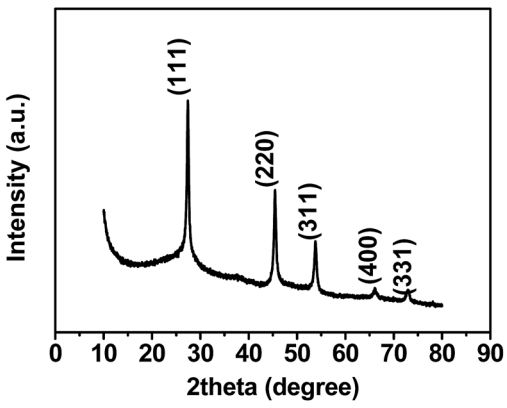

Fig. 1 XRD pattern of the porous amorphous Ge/C composites.

[a]Key Laboratory for Micro-/Nano-Optoelectronic Devices of Ministry of Education, School of Physics and Electronic Science, Hunan University, Changsha 410082, China. E-mail: nanoelechem@hnu.edu.cn

[b]College of Chemistry and Chemical Engineering, Anyang Normal University, Anyang, 455000 Henan, China. E-mail: guowei810807@163.com

[c]Institute for Superconducting and Electronic Materials, University of Wollongong, Wollongong, Australia

† Electronic supplementary information (ESI) available. See DOI: 10.1039/c5ra02459e

Ge content in porous amorphous Ge/C composites is calculated to be 62.6%, based on the weight loss upon carbon combustion and the oxidizing conversion of Ge to GeO_2 in air.

The morphology of porous amorphous Ge/C composites was characterized by transition electron microscope (TEM), and further mapped through TEM and energy-dispersive X-ray spectroscopy (EDS) by displaying the integrated intensity of Ge and C signals as a function of the beam position when operating the TEM in scanning mode (STEM). Fig. 2a and b show the whole morphology of the porous amorphous Ge/C composites, which indicate that the sample is composed the assembled particles. In magnified TEM image (Fig. 2c), one could not discriminate between C and Ge. The magnified TEM image in Fig. 2d indicates there are no crystalline Ge nanoparticles. To confirm the distribution of Ge and C components in the composites, element mapping analysis was conducted. Fig. 2e displays high-angle annular dark field scanning TEM (HAADF-STEM) image of the as-obtained porous amorphous Ge/C composites, which also indicate the porous characteristics of the composites. The mapping results (Fig. 2f and g) reveal that C and Ge are distributed homogeneously in the composites. Moreover, the BET surface area of porous amorphous Ge/C composites was measured to be 38.4 $m^2\ g^{-1}$, and their porous size distribution mainly ranges from 3.5 to 17 nm, as shown in Fig. S2.†

The formation process of porous amorphous Ge/C composites involves two steps: (i) dissolve GeO_2 into oleic acid by ethylenediamine (en), and then evaporate the en; (ii) reduce and carbonize the GeO_2/oleic acid precursors in the Ar/H_2 atmosphere at 650 °C. The first step is extremely important to obtain small particles of Ge from large GeO_2 microparticles (Fig. S3†). During the second step, oleic acid could be carbonized into amorphous carbon,[34,35] and GeO_2 was reduced to Ge by hydrogen at the same time. Oleic acid play triple roles: inhibiting the growth of Ge nanoparticles; providing C resource for the formation of the amorphous C, facilitating the formation of pores during the release of gases. In virtue of composites and porous structure, the porous amorphous Ge/C composites are expected to show promising electrochemical performance as anode materials for lithium-ion batteries.

Fig. 3 shows the typical CV curves for the porous amorphous Ge/C composites. The cathodic peak (0.06–0.15 V) was ascribed to the alloying process of Ge to $Li_{4.4}Ge$, respectively. The anodic peaks (0.41 and 0.56 V) were attributed to the de-alloying process of $Li_{4.4}Ge$. These results are well in agreement with the lithiation/delithiation processes in the GeO_x/reduced graphene oxide (GeO_x/RGO) composite.[36] Compared to the reported Ge/C composites synthesized by a tandem plasma reaction method, the lithiation/delithiation voltages were obviously lowered.[33] Moreover, some irreversible capacity observed in the first cycle could be attributed to the formation of the solid electrolyte interface (SEI) in the voltage range (0–0.8 V), which is also lower than the reported literature.[33] Moreover, the irrepressible capacity might be originated from to the decomposition of the electrolyte. Clearly, the electrochemical characteristics of the similar materials are strongly determined by their synthetic methods. In addition, the irreversible peak gradually disappears along with the cycling in the subsequent cycles. The CV curves of the following cycles are almost overlapped, indicating high reversibility of Ge in the composite and good overall cycling stability.

The rate ability and cycling performance of porous amorphous Ge/C composites were evaluated between 0.01 and 3.0 V (*vs.* Li/Li^+) by gradually increasing the current rate step-wise from 200 mA g^{-1} to 6400 mA g^{-1}, and then returning back to 200 mA g^{-1} with long cycles. Fig. 4a shows the voltage profiles of porous amorphous Ge/C composites at various current densities. The characteristics of charge/discharge curves are similar to the results of reported Ge/C composites. The polarization was obviously increased with increasing current density, which is accorded with the GeO_x/reduced graphene oxide (GeO_x/RGO) composite.[36]

Fig. 4b and S4† show the plots of the charge/discharge capacity and Coulombic efficiency *versus* cycle number for the

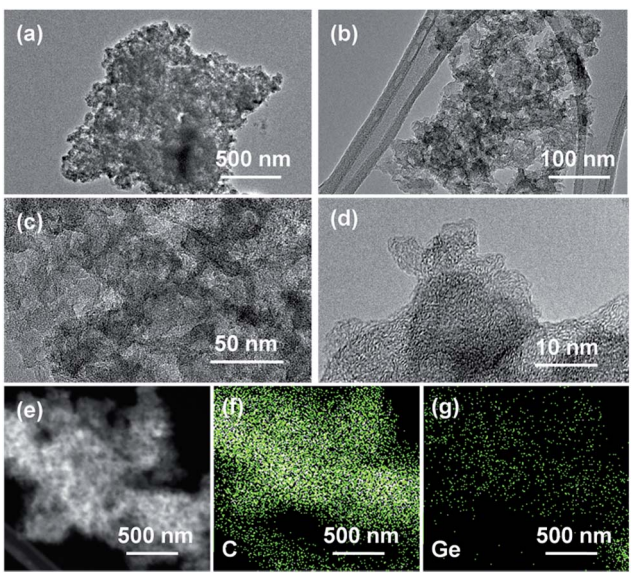

Fig. 2 (a–d) TEM images, (e) HAADF-STEM image (e) and XRD pattern of porous amorphous Ge/C composite, (f and g) corresponding C and Ge elemental maps.

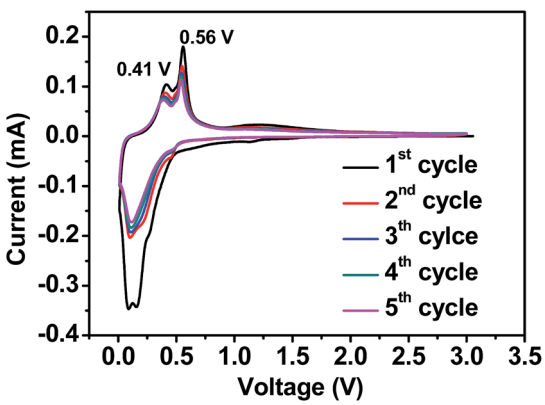

Fig. 3 CV curves of porous amorphous Ge/C composites at a rate of 0.05 mV s^{-1} for first 5 cycles.

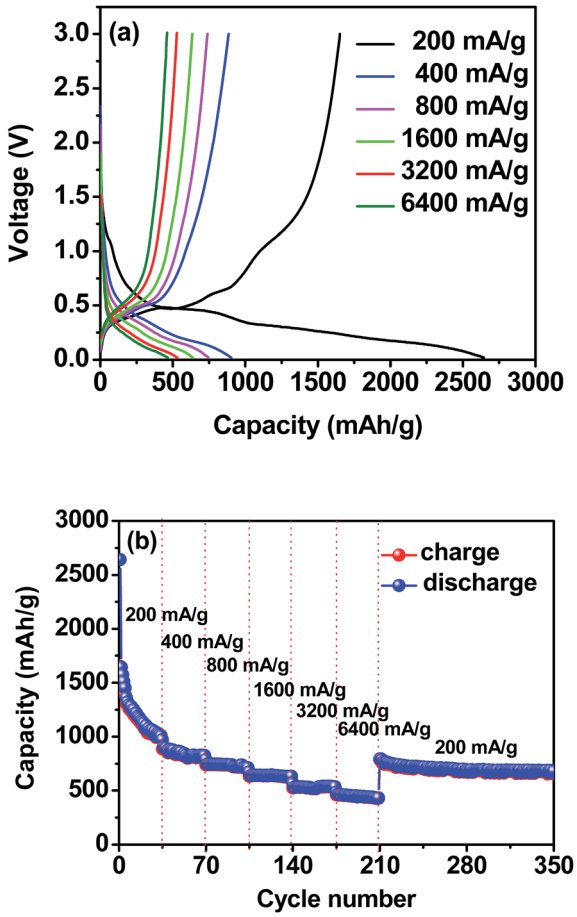

Fig. 4 (a) Typical charge/discharge curves and (b) rate capability and cycling performance of the porous amorphous Ge/C composites at various current densities.

porous amorphous Ge/C composites, respectively. As shown in Fig. 4b, one can find that there is a capacity-decreasing trend with increasing current rates. This is due to that the electron transport becomes the limiting step in the lithiation/delithiation processes when current density increases dramatically. The porous amorphous Ge/C composites deliver reversible capacities of 836, 724, 630, 535 and 450 mA h g^{-1} at 400, 800, 1600, 3200 and 6400 mA g^{-1}, respectively. The electrode can deliver a reversible capacity of ~681 mA h g^{-1} after 350 cycles at a current density of 200 mA g^{-1}, even undergoing long cycles at higher current densities. As shown in Fig. S4,† the Coulombic efficiency almost keeps above 98%, except several cycles when current densities were changed.

The porous amorphous germanium/carbon composites have demonstrated to take excellent electrochemical properties in cycling life and rate ability. The long cycling life and good rate ability of porous amorphous germanium/carbon composites are attributed to good electronic conduction of amorphous carbon matrix, short Li insertion distances due to smaller particles, high interfacial contact area with electrolyte due to their porous structure and large BET area, which originate from the unique structure of germanium/carbon composites.

In conclusion, we have successfully developed an effective synthetic route to obtain porous amorphous Ge/C composites for lithium-ion batteries. The unique structural features of the porous amorphous Ge/C composites such as the electrically conducting of carbon networks and porous structure, make them promising as anode materials for next-generation LIBs. Moreover, we expect that our method could be extended to prepare other functional composite materials in future.

Acknowledgements

This work was supported by the National Natural Science Foundation of China (Grant no. 51302078 and 51302079).

Notes and references

1 P. Poizot, S. Laruelle, S. Grugeon, L. Dupont and J.-M. Tarascon, *Nature*, 2000, **407**, 496–499.
2 J. M. Ma, J. B. Lian, X. C. Duan, X. D. Liu and W. J. Zheng, *J. Phys. Chem. C*, 2010, **114**, 10671–10676.
3 Y. J. Chen, J. M. Ma, Q. H. Li and T. H. Wang, *Nanoscale*, 2013, **5**, 3262–3265.
4 B. Wang, X. L. Wu, C.-Y. Shu, Y.-G. Guo and C.-R. Wang, *J. Mater. Chem.*, 2010, **20**, 10661–10664.
5 L. Zhang, H. B. Wu and X. W. Lou, *J. Am. Chem. Soc.*, 2013, **135**, 10664–10672.
6 Y. Cai, X. Li, L. Wang, H. Y. Gao, Y. N. Zhao and J. M. Ma, *J. Mater. Chem. A*, 2015, **3**, 1396–1399.
7 X. Li, J. T. Xu, L. Mei, Z. J. Zhang, C. Y. Cui, H. K. Liu, J. M. Ma and S. X. Dou, *J. Mater. Chem. A*, 2015, **3**, 3257–3260.
8 Y. J. Mai, S. J. Shi, D. Zhang, Y. Lu, C. D. Gu and J. P. Tu, *J. Power Sources*, 2012, **204**, 155–161.
9 N. Liu, L. B. Hu, M. T. McDowell, A. Jackson and Y. Cui, *ACS Nano*, 2011, **5**, 6487–6493.
10 W. J. Li, S.-L. Chou, J.-Z. Wang, J. H. Kim, H.-K. Liu and S. X. Dou, *Adv. Mater.*, 2014, **26**, 4037–4042.
11 D.-J. Xue, S. Xin, Y. Yan, K.-C. Jiang, Y.-X. Yin, Y.-G. Guo and L.-J. Wan, *J. Am. Chem. Soc.*, 2012, **134**, 2512–2515.
12 Z. P. Guo, Z. W. Zhao, H. K. Liu and S. X. Dou, *Carbon*, 2005, **43**, 1392–1399.
13 L. Y. Lim, N. Liu, Y. Cui and M. F. Toney, *Chem. Mater.*, 2014, **26**, 3739–3746.
14 G. Cui, L. Gu, L. Zhi, N. Kaskhedikar, P. A. van Aken, K. Müllen and J. Maier, *Adv. Mater.*, 2008, **20**, 3079–3083.
15 T. Song, H. Cheng, H. Choi, J. H. Lee, H. Han, D. H. Lee, D. S. Yoo, M. S. Kwon, J. M. Choi, S. G. Doo, H. Chang, J. Xiao, Y. Huang, W. I. Park, Y. C. Chung, H. Kim, J. A. Rogers and U. Paik, *ACS Nano*, 2012, **6**, 303–309.
16 X.-L. Wang, W.-Q. Han, H. Chen, J. Bai, T. A. Tyson, X.-Q. Yu, X.-J. Wang and X.-Q. Yang, *J. Am. Chem. Soc.*, 2011, **133**, 20692–20695.
17 Y. D. Ko, J. G. Kang, G. H. Lee, J. G. Park, K. S. Park, Y. H. Jin and D. W. Kim, *Nanoscale*, 2011, **3**, 3371–3375.
18 L. Shen, X. Guo, X. Fang, Z. Wang and L. Chen, *J. Power Sources*, 2012, **213**, 229–232.

19 N. G. Rudawski, B. R. Yates, M. R. Holzworth, K. S. Jones, R. G. Elliman and A. A. Volinsky, *J. Power Sources*, 2013, **223**, 336–340.
20 M. H. Seo, M. Park, K. T. Lee, K. Kim, J. Kim and J. Cho, *Energy Environ. Sci.*, 2011, **4**, 425–428.
21 B. Li, H. Cao, J. Shao and M. Qu, *Chem. Commun.*, 2011, **47**, 10374–10376.
22 H. Li, Z. X. Wang, L. Q. Chen and X. J. Huang, *Adv. Mater.*, 2009, **21**, 4593–4607.
23 D. T. Ngo, R. S. Kalubarme, H. T. T. Le, J. G. Fisher, C.-N. Parkl, I.-D. Kim and C.-J. Park, *Adv. Funct. Mater.*, 2014, **24**, 5291–5298.
24 M. X. Liu, X. M. Ma, L. H. Gan, Z. J. Xu, D. Z. Zhu and L. W. Chen, *J. Mater. Chem. A*, 2014, **2**, 17107–17114.
25 C. H. Yao, J. Wang, H. F. Bao and Y. F. Shi, *Mater. Lett.*, 2014, **124**, 73–76.
26 S. L. Li, C. Chen, K. Fu, R. White, C. X. Zhao, P. D. Bradford and X. W. Zhang, *J. Power Sources*, 2014, **253**, 366–372.
27 J. Hao, X. X. Liu, N. Li, X. S. Liu, X. X. Ma, Y. Zhang, Y. Li and J. P. Zhao, *RSC Adv.*, 2014, **4**, 60371–60375.
28 S. Fang, L. F. Shen, H. Zheng and X. G. Zhang, *J. Mater. Chem. A*, 2015, **3**, 1498–1503.
29 Y. Xiao and M. H. Cao, *ACS Appl. Mater. Interfaces*, 2014, **6**, 12922–12930.
30 J. W. Qin, X. Wang, M. H. Cao and C. W. Hu, *Chem.–Eur. J.*, 2014, **20**, 9675–9682.
31 J. X. Cheng, J. Q. Wang, W. H. Li, X. W. Liu and Y. Yu, *RSC Adv.*, 2014, **4**, 37746–37751.
32 G. H. Yue, X. Q. Zhang, Y. C. Zhao, Q. S. Xie, X. X. Zhang and D. L. Peng, *RSC Adv.*, 2014, **4**, 21450–21455.
33 W. Li, J. Zheng, T. K. Chen, T. Wang, X. J. Wang and X. G. Li, *Chem. Commun.*, 2014, **50**, 2052–2054.
34 G. Zhou, J. M. Ma and L. B. Chen, *Electrochim. Acta*, 2014, **133**, 93–99.
35 D. N. Lei, T. Yang, B. H. Qu, J. M. Ma, Q. H. Li, L. B. Chen and T. H. Wang, *Sustain. Energ.*, 2014, **2**, 1–4.
36 D. P. Lv, M. L. Gordin, R. Yi, T. Xu, J. X. Song, Y.-B. Jiang, D. Choi and D. H. Wang, *Adv. Funct. Mater.*, 2014, **24**, 1059–1066.

